Civil Engineering Dimension
https://ced.petra.ac.id

Evaluation of Infiltration Models with Double Ring Infiltrometer Test on Residual Soil in Kulonprogo, Indonesia

Muntohar, A.S.[1]*, Ikhsan, J.[1], Setiati, R.[1,2], and Uzuoka, R.[3]
[1] Landslide Research Center, Universitas Muhammadiyah Yogyakarta, INDONESIA
[2] Former Master Student of Department of Civil Engineering, Universitas Andalas, West Sumatera, INDONESIA
[3] Disaster Prevention Research Institute, Kyoto University, JAPAN

DOI: https://doi.org/10.9744/ced.27.2.193-204

Article Info:
Submitted: Jan 26, 2025
Reviewed: Feb 24, 2025
Accepted: May 13, 2025

Keywords:
double ring infiltrometer,
infiltration rate,
hydraulic conductivity,
Green–Ampt,
Kostiakov,
Horton,
Philips equations.

Corresponding Author:
Muntohar, A.S.
Landslide Research Center,
Universitas Muhammadiyah Yogyakarta,
INDONESIA
Email: muntohar@umy.ac.id

Abstract

The hydraulic conductivity of soil is an essential parameter for evaluating the slope instability triggered by rain infiltration. This research uses a Double-Ring Infiltrometer (*DRI*) at five locations to estimate the hydraulic conductivity from a field infiltration test. Four infiltration models were examined to estimate hydraulic conductivity, including Green–Ampt, Kostiakov, Horton, and Philips equations. Curve fitting on the infiltration rate–time plots were computed with the least square error to determine the infiltration parameters using Levenberg–Marquardt algorithm. The basic infiltration rate ranges from 6.88 mm/h to 721.5 8 mm/h. The Horton and Philips infiltration model provides better statistical performance to estimate the infiltration rate. The estimated hydraulic conductivity from the four infiltration models results in a relative convergence value; however, the estimation results in more biased hydraulic conductivity at locations containing clay fraction and high-plasticity silt, especially for Green–Ampt and Philip infiltration models.

INTRODUCTION

Many landslides in Indonesia occur during the rainy season [1,2]. In the dry season, the soil is in an unsaturated condition. Entering the rainy season, rainwater infiltration into the soil surface causes the soil pores to be filled with water and become saturated. Rain infiltration into the soil can cause an increase in pore water pressure and reduce shear strength [3,4]. Furthermore, the soil mass increases and triggers soil movement [2,5]. Thus, the time of occurrence of the landslide was determined by the rate and depth of rain infiltration below the slope surface and additional factors such as morphology, geology, and slope geotechnics [6].

Field infiltration tests are paramount to determining infiltration rate and depth during rainfall. The infiltration test is always closely related to the saturated soil hydraulic conductivity (k_s). The infiltration equation proposed by Green and Ampt [7], Kostiakov [8], and Philips [9] directly provides a relationship between infiltration and saturated soil hydraulic conductivity. There are several types of field tests to determine the infiltration rate and hydraulic conductivity of the soil in the field, including double ring infiltrometer [10], Modified Philip Dunne Infiltrometer Test [11], mini disc infiltrometer [12], bucket-sized infiltration ring [13]. Compared to the tension disc infiltrometer, the Double Ring Infiltrometer (DRI) is a more economical way to measure the saturated hydraulic conductivity of topsoil. The steady-state infiltration rate measured by DRI is often equal to the saturated hydraulic conductivity of the soil [14]. However, the steady-state condition might be achieved in a relatively long observation period [15]. Although the DRI can determine the saturated hydraulic conductivity, Yolcubal et al. [16] stated that the estimated saturated hydraulic conductivity value from *DRI* is too high compared to the tension disc infiltrometer test.

Note : Discussion is expected before November, 1st 2025, and will be published in the "Civil Engineering Dimension", volume 28, number 1, March 2026.
ISSN : 1410-9530 print / 1979-570X online
Published by : **Petra Christian University**

Studies on infiltration tests using DRI on slopes have not been widely explored. Previous studies, such as those conducted by Wahyu et al. [17] and Octariko and Budianta [18], used the results of infiltration tests in the field to determine the hydraulic conductivity value for agricultural and groundwater geology purposes. Infiltration tests on slopes can be used to determine saturated hydraulic conductivity (k_s), which is identified as a controlling parameter for slope instability triggered by rain infiltration. Many studies on rainfall-induced landslides determine the k_s from the laboratory test which the condition is limited to the specimen size and sample quality. The hydraulic conductivity will greatly determine the slope stability triggered by rainwater infiltration, especially in Kulonprogo, where the slopes were predominantly covered with volcanic residual soil [1]. Typically, the volcanic residual soil was resulted from the weathered andesitic breccia and tuffs. For this reason, a study is needed to evaluate the hydraulic conductivity from the DRI tests. This study uses the DRI method to determine the infiltration characteristic of residual soil on slopes in Kulonprogo. The infiltration models can estimate the final infiltration or steady state condition corresponding to saturated hydraulic conductivity. Slope stability was affected by the rainwater redistribution, in which the saturated hydraulic conductivity firmly controlled the rainwater transmission during infiltration [19]. The objectives of this study are (1) to determine the final infiltration rate, (2) to evaluate the suitable infiltration model for the test results, and (3) to estimate the saturated hydraulic conductivity of soil. The investigation results can be applied to evaluate the effect of the variability of hydraulic conductivity on slope stability for forthcoming research.

METHODS

Location of Study

The study was conducted on the slopes around the main Kalibawang irrigation channel in Banjararum, Kalibawang District, Kulonprogo Regency, Yogyakarta province (Figure 1). The slope varies from 18° to 25°. The area was characterized as an active landslide area and classified as slow movement (creep) [20-22]. The failure zone in 2002 and slow movement in 2002 and 2015 are also indicated in Figure 1. The land cover of the area was *Pennisetum purpureum* grass with a 1-1.5 m height. The slope area was laid on the Kebobutak formation, which was an old andesite formation. The geological formation consists of tuffaceous andesitic breccia and tuffs. Colluvial deposits such as clayey silt, sandy silt, and silt were characterized as the result of weathering of the parent rock [20].

There were five test point locations, as shown in Figure 1. The experiment was conducted on 3 March 2017. The weather was clear during the test, but light rainfall with an average intensity of 4 mm/h and 1.5 mm/h occurred two days before the test. The initial water content on the soil surface to a depth of 10 cm was measured at 52.6%, 47.9%, 45.3%, 57.1%, and 48.7%, respectively, in sequence at KP-1 to KP-5. Based on the Unified Soil Classification System, the soil at the test site was identified as fine-grained soil because more than 50% of the particles are finer than 0.075 mm, as shown in the grain size distribution curve in Figure 2a. The soil samples were comprised of 65.9% – 79% silt, 8.6% – 12.8% clay, and 9% – 25.5% sand fractions (see Figure 2a). The clay fraction was determined as particle size less than 2mm. The soils were classified into two groups: (1) low plasticity silt (ML) at KP-1, KP-2 and KP-3, and (2) high plasticity silt (MH) at KP-4, and KP-5. In addition, textural classification is commonly used to indicate infiltrability [23]. According to USDA-SCS, the soil at the test site has a silt-loam texture (KP-2 and KP-3) and silt texture at KP-1, KP4, and KP-5 (see Figure 2b).

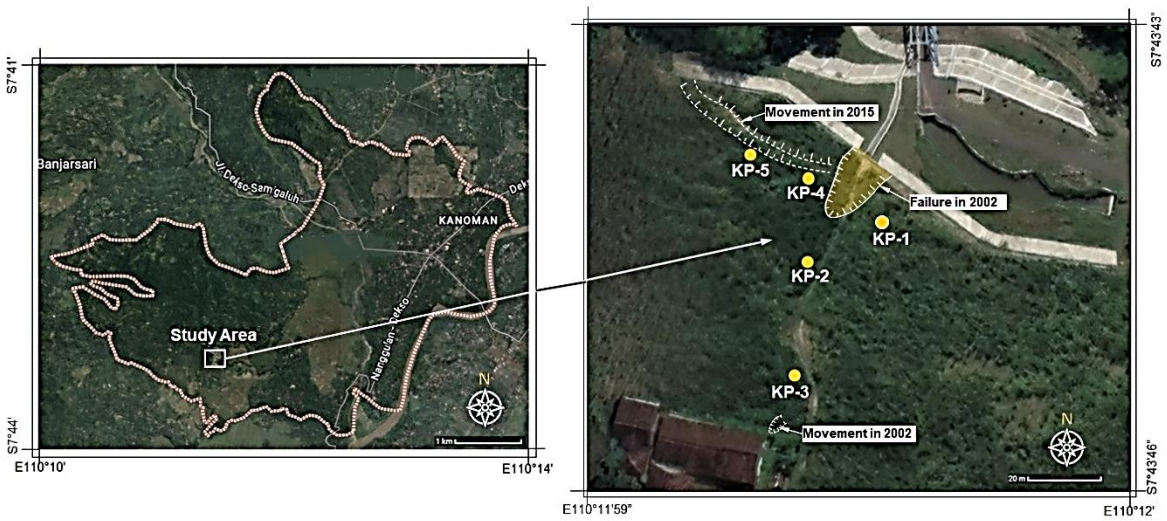

Figure 1. Location of the Study, Testing Points, and Soil Sampling

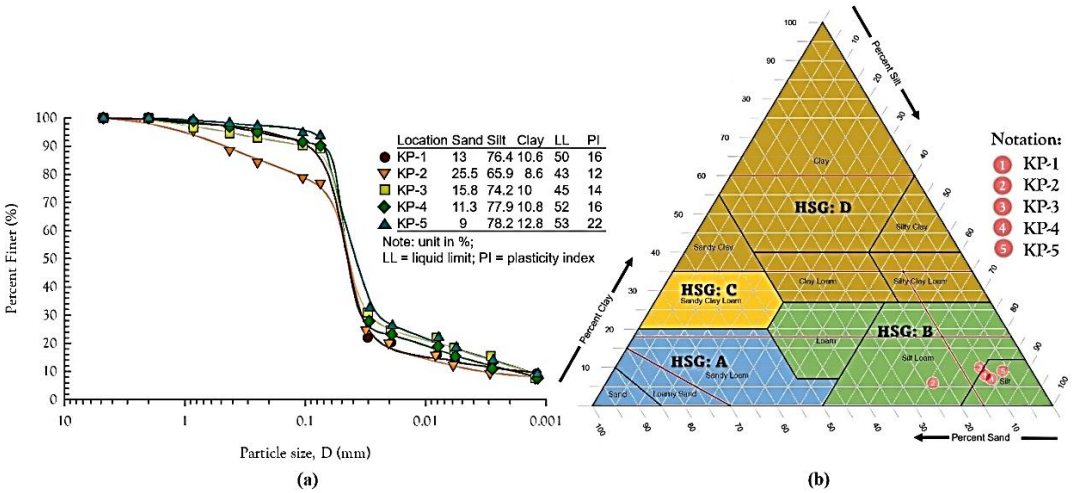

Figure 2. (a) Particles Size Distribution Curve, (b) Soil Texture Classification of USDA-SCS

Equipment and Testing Procedure

The main equipment used for testing infiltration capacity in the field in this study was a double-ring infiltrometer consisting of two pairs of concentric cylinders or tubes or inner (cylinder B) and outer cylinders (cylinder A). The outer cylinder has a diameter of 55 cm, and the inner cylinder has a diameter of 30 cm with a height of 25 cm. Figure 3 shows the installed DRI and the apparatus in the field. The infiltration test was conducted following the procedure in ASTM D3385-09 [24]. The cylinder was placed on a flat ground surface and inserted with a hammer to a depth of 10 cm below the surface to prevent water seepage from inside the cylinder. Water was poured into cylinder A as high as 5-10 cm for 2 minutes, and the water level was kept constant. Then, water was poured into cylinder B, and the water level was kept higher than in cylinder B. The water level decrement (ΔH) in cylinder B was measured every 2-minute time interval (Δt) for 40-60 minutes, or there was no change in water level, or it remained constant. The cumulative water level decrement at time t was recorded as cumulative infiltration $F(t)$, calculated by Equation 1. The infiltration rate at time t was determined by Equation 2.

$$F(t) = \sum_{i=0}^{i=t} \Delta H_i \tag{1}$$

$$f(t) = \frac{\Delta H}{\Delta t} \tag{2}$$

where ΔH is the water level height (cm) at time interval Δt (minutes), $F(t)$ and $f(t)$ are cumulative infiltrations and infiltration rate at time t, respectively.

After the infiltration test was completed, soil samples were collected using a hand boring at every depth of 10 cm, 20 cm, 30 cm, 40 cm, and 50 cm. The soil samples at each depth were tested to determine soil moisture. The testing procedure followed the SNI 1965:2008 [25].

Figure 3. Double Ring Infiltrometer Set Up in the Field

Table 1. The Infiltration Equations from Several Models

Infiltration Model	Equations	Parameter	
Green-Ampt:	$f(t) = k_s\left(1+\frac{\Delta\theta\psi_f}{F(t)}\right)$	k_s, Dq, y_f	(3)
	$F(t) - \Delta\theta\psi_f \ln\left(1+\frac{F(t)}{\Delta\theta\psi_f}\right) = k_s \cdot t$		(4)
Kostiakov:	$f(t) = K \cdot t^{-\alpha}$	a, K	(5)
Horton:	$f(t) = f_c + (f_o - f_c)e^{-\lambda t}$	l, f_c, f_o	(6)
Philips:	$f(t) = \frac{1}{2} S \cdot t^{-1/2} + K_\theta$	S, K_θ	(7)

Notation:
F(t) = cumulative infiltration at time-t (mm), $f(t)$ = infiltration rate at time-t (mm/h);
f_c = final infiltration rate or infiltration capacity (mm/h); f_o = initial infiltration rate (mm/h);
l = constant in Horton's infiltration model; t = time (h); Δt = time interval (h), S = sorptivity (mm.h$^{-1/2}$); K_θ = transmissivity term in Philip's infiltration model; K = constant in Kostiakov's infiltration model; a = constant in Kostiakov's infiltration model; $\Delta\theta$ = volumetric soil moisture deficit = $\theta_s - \theta_i$, ; θ_s and θ_r = the saturated and residual soil moisture, respectively; ψ_f = suction head at wetting front (mm); k_s = saturated hydraulic conductivity (mm/h)

Data Analysis and Determination of Infiltration Parameters

The relationship between infiltration rate and time was plotted in a graph to estimate the infiltration capacity. The results of soil infiltration rate measurements in the field were analyzed to estimate the soil infiltration rate based on four equation models, including Green-Ampt [7], Kostiakov [8], Horton [26], and Philips [9]. The infiltration rate equations are written in Table 1. The parameters of each infiltration equation were determined by fitting them on the plot of infiltration rate – time. The best curve-fitting was computed based on the least squares error. This algorithm seeks the values of the parameters that minimize the sum of the squared differences between the values of the observed and predicted values of the dependent variable. The Marquardt-Levenberg algorithm was used to find the coefficients (parameters in Table 1) of the independent variables that give the "best fit" between the equation and the data [27]. Performance of the predictors in infiltration model was evaluated by statistical indicators such as coefficient of determination (R^2), root mean square error (*RMSE*), and normalized root mean square error (*NRMSE*) [28]. The range of R^2 is 0 – 1, and R^2 = 1 indicates a stronger explanatory power of the model. A small value of *RMSE* and *NRMSE* value close to 0 identifies a numerical simulation in good agreement with the field observations [28].

RESULTS AND DISCUSSION

Infiltration Rate

The relationship between infiltration rate and time is presented in Figure 4. The results show that the infiltration rate will decrease with increasing time. The infiltration rate generally decreases rapidly within 12 minutes (0.2 hours), then decreases asymptotically with elapsed time. As time increases, the infiltrated water will moisten the soil layer, and the soil reaches a saturated state. Thus, the soil can no longer absorb water. Thus, the infiltration rate decreases asymptotically. However, the soil is a porous medium, so water will flow into deeper soil layers.

In principle, the infiltration rate measures the velocity of water on the soil surface entering downward to the subsurface. Infiltration rate is water flow through dry or partially saturated soil pores. The infiltration rate will be steady when the volume of pores space is filled with water. This final infiltration rate (f_c) is related to hydraulic conductivity. The final infiltration rate results from the DRI test show that the infiltration rate varies over time for each test location. The final infiltration rate, if sorted from the highest, occurred at locations KP-2 (721.5 mm/h), KP-3 (276 mm/h), KP-1 (88 mm/h), KP-5 (51 mm/h), and the lowest at location KP-4 (12 mm/h). The final infiltration rate may not have shown a constant (steady state) value. Therefore, the infiltration capacity can be computed from the infiltration equation, representing the saturated soil conductivity. Figure 5 plots the curve fitting of the four infiltration equations on the relationship between infiltration rate and time from the DRI test. The curve fitting results are infiltration equation parameters, as presented in Table 2. The statistical indicators for evaluating the performance

of each infiltration model are figured in Figure 6. The estimated average values of coefficient of determination (R^2) are 0.956, 0.955, 0.967, 0.957; and the root mean square error (*RMSE*) values are 5.582, 4.337, 4.104, 3.6 mm/h, and normalized root mean square error (*NRMSE*) values are 0.062, 0.052, 0.048, 0.041 for Green – Ampt, Kostiakov, Horton, and Philips model respectively. The Horton and Philips infiltration model provides a better infiltration model, which results in the highest R^2 and smaller *NRSME*. These results dealt with research conducted by Su et al. [29], Ketsela et al. [30], Mesele et al. [31].

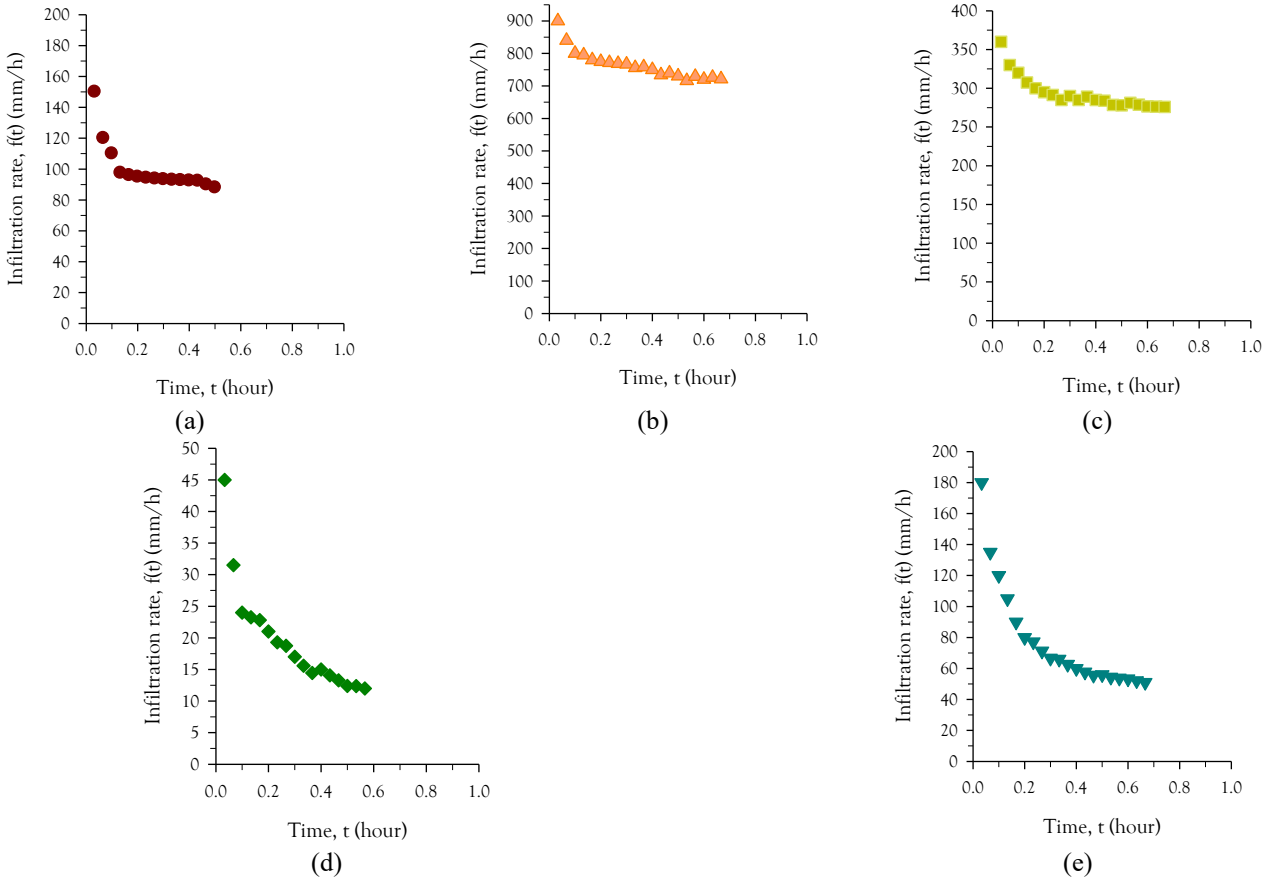

Figure 4. Variation of Infiltration Rate and Time of DRI Test Results at Test Points (a) KP-1, (b) KP-2, (c) KP-3, (d) KP-4, (e) KP-5

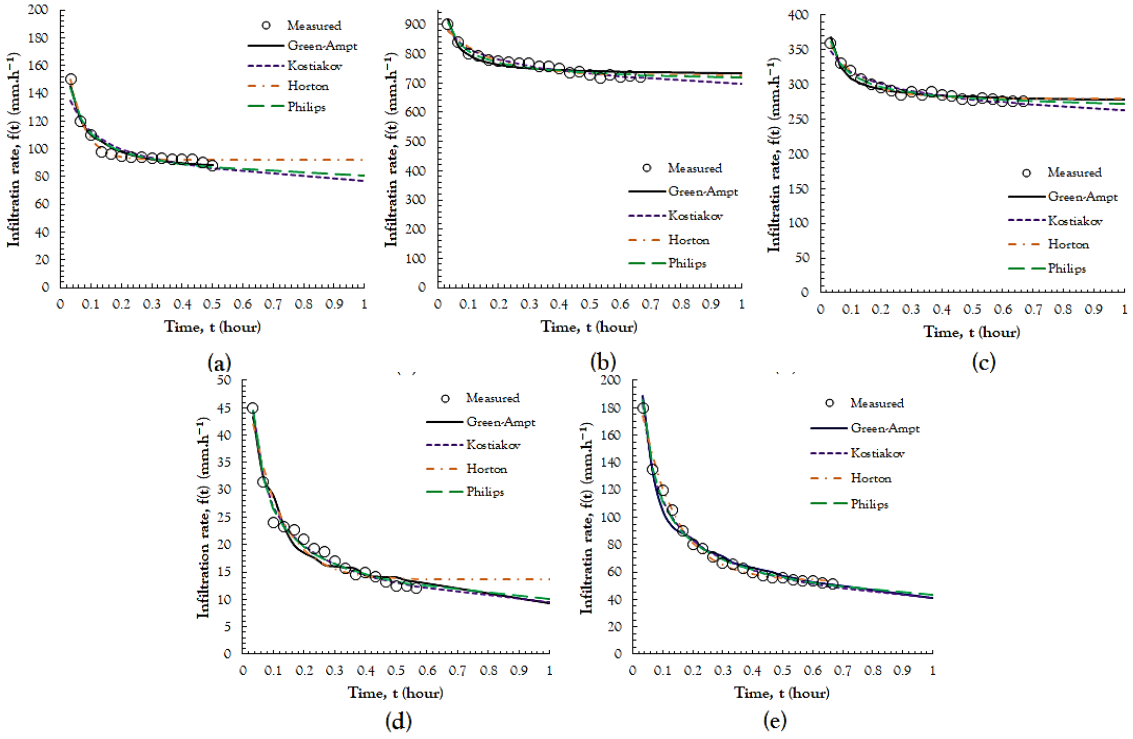

Figure 5. Curve Fitting of Infiltration Model at Various location (a) KP-1, (b) KP-2, (c) KP-3, (d) KP-4, (e) KP-5

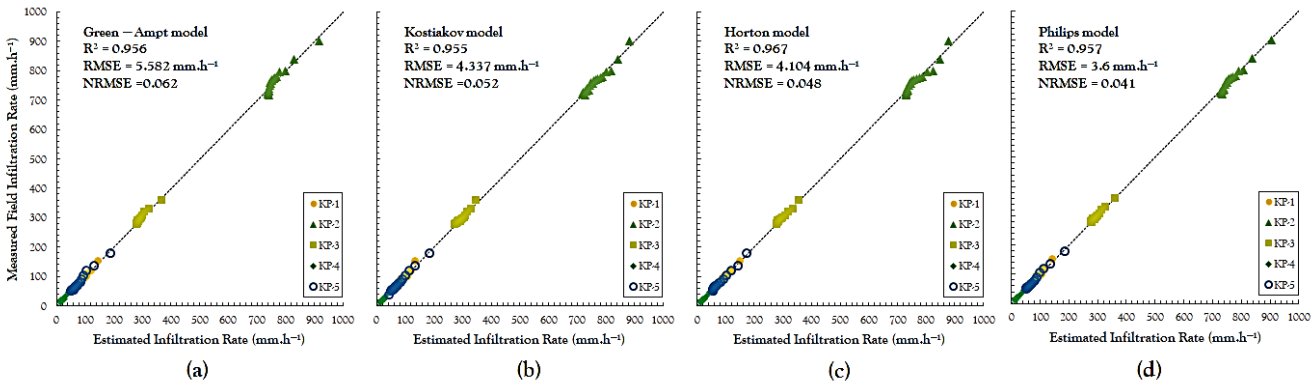

Figure 6. Correlation between Measured and Estimated Infiltration Rate and Statistical Indicators for Performance Evaluation of Infiltration Models (a) Green–Ampt, (b) Kostiakov, (c) Horton, (d) Philips

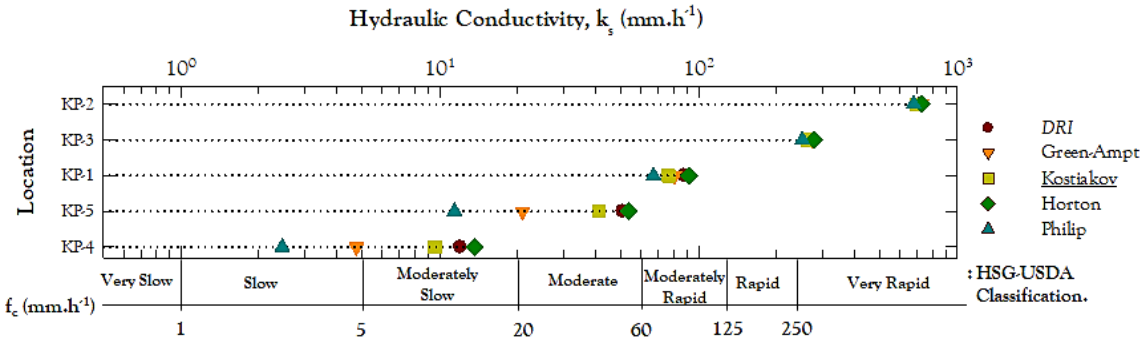

Figure 7. Variation of the Estimated Hydraulic Conductivity and Classification

Table 2. Infiltration Parameter for Various Infiltration Model obtained from the Best Fit

Infiltration Model	Parameter	Unit	Test Location				
			KP-1	KP-2	KP-3	KP-4	KP-5
Green-Ampt	k_s	mm/h	80.7	725	274	4.76	20.9
	y_f	mm	70.9	141	72.8	214	473
	Dq *		0.216	0.125	0.164	0.057	0.102
Kostiakov	K	mm/h	76.5	698	263	9.59	41.2
	a		0.166	0.069	0.083	0.449	0.438
Horton	l	1/h	19.8	6.75	9.64	9.91	8.78
	f_o	mm/h	203	917	385	53.1	215
	f_c	mm/h	91.9	726	279	13.6	53.7
Philips	K_θ	mm/h	66.9	677	252	2.46	11.4
	S	mm/h$^{1/2}$	28.2	83.5	40.2	15.3	63.4
Field measured	f_c	mm/h	88	721.5	276	12	51

Note: * Dq was measured from the soil moisture samples before and after test

Estimation of Hydraulic Conductivity

In Table 2, the Horton infiltration model directly calculates the steady infiltration rate as expressed as infiltration capacity (f_c). For each infiltration model, the f_c value is defined by the value of k_s in the Green – Ampt model, K in the Kostiakov model, and K_θ in the Philips infiltration equation. Figure 7 presents the variation of saturated hydraulic conductivity. The logarithmic scale is applied to exhibit a noticeable bias, particularly in Green–Ampt and Philips models. The results of this plotting indicate that the estimated hydraulic conductivity from the four infiltration models is relatively convergent for silt–loam texture at locations KP-2 (698 – 726 mm/h) and KP-3 (252 – 279 mm/h). However, for silt texture, the estimated k_s is relatively convergent at KP-1 (66.9 – 91.9 mm/h), but the k_s is more biased at locations KP-4 (2.46 13.6 mm/h) and KP-5 (11.4 – 53.7 mm/h), especially the estimation from the Green – Ampt and Philip infiltration models. Bias or large variability of saturated hydraulic conductivity leads to slope stability being uncertain [19].

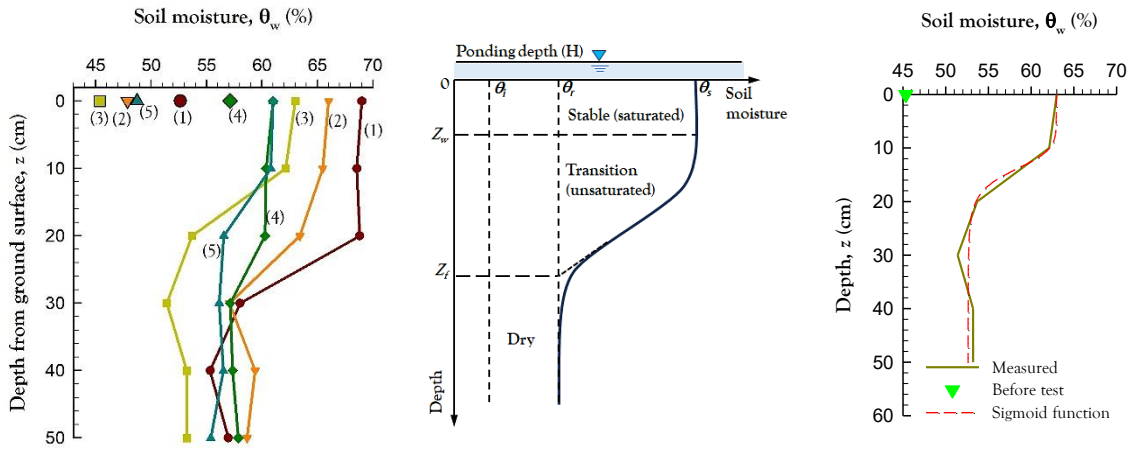

(a) (b) (c)

Figure 8. Soil Moisture Profile (a) Distribution of Soil Water Related to Depth after Testing (Note: Numbers 1 – 5 indicate the test location, symbols ■◆●▲▼ indicate initial soil moisture, lines-symbols indicate water content after testing) (b) Simplified Distribution of Soil Moisture, (c) Sigmoidal Model for Soil Moisture Profile at KP-3

Distribution of Soil Moisture

Changes in soil moisture can validate the water infiltration rate into the soil layer. Figure 8a presents the profile of soil water content and depth. Figure 8a also plots the initial soil water content at the soil surface before the test began. The initial soil moisture at the ground surface is 52.6%, 47.9%, 45.3%, 57.1%, and 48.7%, respectively, at KP-1 to KP-5. At the beginning of infiltration, water enters the partially saturated porous media, the voids are filled, and flow occurs. As infiltration continues, flow occurs between the ponding on the surface and the surface of the wetting front. Soil moisture increases with time as the infiltrated water increases through the wetting front (see Figure 8a). The wetting front is an indicator that confirms the actual cumulative infiltration. Thus, it was related to determining the saturated hydraulic conductivity [29]. According to Darcy's equation for vertical flow system, the infiltration rate (f) is dependent to K_s, Z_f, suction at wetting front (y_f), and ponding depth (H) (see Figure 8b). Bower (1989) formulated the equation as $f \cdot Z_f = K_s\left(H + Z_f - \psi_f\right)$. The results of the Bodman and Colman [32] wetting front study were simplified by Yao et al. [33], which has two patterns, namely the stable part (saturated) and the transition part (unsaturated) (see Figure 8b). Yao et al. (2022) approached the transition part with an elliptic equation. However, in this study, changes in water content with depth can be modeled as a sigmoidal form, as shown in Figure 8b. Mathematically, the sigmoidal function equation is written as follows:

$$\theta(z,t) = \theta_r + \frac{(\theta_s - \theta_r)}{1 + \left(\frac{z}{z_o}\right)^b} \tag{8}$$

Where $\theta(z,t)$ is the soil water content at depth z at time t (the end of the test), $(\theta_s - \theta_r)$ is the soil moisture deficit, θ_s and θ_r are the saturated and residual soil moisture respectively, z_o is the midpoint value of depth, b is a constant represents the growth rate. Figure 8c shows the soil moisture profile with the sigmoidal function.

The soil moisture profile shows that the wetting front depth (Z_f) can reach 30 cm deep at KP-1, KP-2, and KP-4 locations. Meanwhile, at locations KP-3 and KP-5, the wetting front reaches 22 cm deep. The stable soil moisture (saturated) depth (Z_w) at KP-1 to KP-5 are 20 cm, 16 cm, 10 cm, 13 cm, and 10 cm, respectively. The soil at KP-2 and KP-3 are classified in a silt-loam texture group, and silt texture is a soil group for KP-1, KP-4, and KP-5 (see Figure 2b). Hence, soil texture does not obviously affect the wetting front or saturated zone depth. The depth of the wetting zone and saturation zones are related to the initial soil moisture conditions. This experiment shows that a higher initial water content tends to reach deeper saturation and wetting zones. However, on the contrary, the depth of the saturation and wetting zone will be shallower at low initial water content.

Discussion

In the *DRI* test, the infiltration rate is measured only in the inner cylinder. This process continues until the infiltration rate becomes stable. The reason for using two cylinders is to reduce the lateral flow divergence under the inner

cylinder resulting from the three-dimensional flow condition so that a truly vertical flow will occur in the inner cylinder [15]. This condition can be achieved by maintaining the same water level in both cylinders, using a large diameter cylinder, and inserting a deeper ring. The depth of the ring inserted below the ground surface was up to 5-15 cm, according to Fatehnia et al. [14], and it can reduce the lateral water flow. However, Lai et al. (2012) stated that the more profoundly the ring was inserted into the soil, the more it would cause disturbance in the soil mass. Thus, the infiltration rate in *DRI* can satisfy the Darcy equation, which considers vertical water infiltration into the ground surface as a piston flow (where the hydraulic conductivity is uniform and the water pressure head on the wetting plane is constant). The water content profile after the DRI test, as in Figure 8a, can confirm whether there is lateral flow or preferential flow in the test. Using the mass balance approach [34] that the total infiltrated water *W(t)* is the same as the cumulative infiltration *F(t)* distributed to a depth of Z_f for infiltration conditions with ponding (see Figure 8b), the total infiltrated water *W(t)* can be formulated as follows:

$$W(t) = \int_{z=0}^{Z_f} \theta(z,t)\, dz \tag{9}$$

At time $t = 0$, the soil moisture at the surface ($z = 0$) is q_i; at the end of the test $t = t_f$, the soil moisture is q_s, decreasing sigmoidal with depth z. If $W(t) < F(t)$, then a nonequilibrium state occurs where the amount of water entering the soil is greater than the water infiltrated in the wetting zone, or drainage occurs [35]. The calculated W(t) is summarized in Table 3 and compared with *F(t)*.

Table 3. Initial Soil Moisture at Ground Surface (θ_{Wi}), Total Infiltrated Water W(T) and Cumulative Infiltration F(T)

Parameter	Location				
	KP-1	KP-2	KP-3	KP-4	KP-5
q_{wi} *(%)*	52.6	47.9	45.3	57.1	48.7
$W(t)$ – mm	54.5	67.7	51.8	8.4	44.1
$F(t)$ – mm	44	481	184	6.8	34

Cumulative infiltration represents the amount of water that enters the soil vertically and flows between the soil pores (diffuse flow) until it reaches the wetting front. Experiments on the soil column model conducted by Ma et al. [36] and Berdouki et al. [37] showed a good agreement between cumulative infiltration and the amount of water infiltrated in the wetting zone. Based on the calculations in Table 3, at locations KP-2 and KP-3, the total infiltrated water W(t) is smaller than the cumulative infiltration *F(t)*, whereas the results for the other three test locations are reversed. Simulations conducted by Lai et al. [38] showed that the depth of the ring inserted into the soil up to 15 cm still allows horizontal flow below the soil mass continuity ring. Thus, cumulative infiltration becomes greater because the water flow into the soil pores was distributed horizontally, especially at locations KP-2 and KP-3. Another possible reason was the occurrence of preferential or finger flow resulting from the left roots of plants [39]. This preferential flow is reasonable because the test location was in *Pennisetum purpureum* grass field area.

The parameters in the Kostiakov and Horton models are generated from regression analysis based on experimental data, so the estimation results are closer to the test data. The Horton and Kostiakov infiltration equations were developed from the curve fitting on measurement results plots that do not represent a robust physical meaning [31]. However, both models have straightforward equations to simulate infiltration, and their parameters are easier to obtain than those of the Philips and Green-Ampt models. Those basic parameters differed from the Green–Ampt and Philips infiltration equations [40], although their parameters can also be determined from fitting. The Philips infiltration model curve fitting has limitations where the K_q or S parameters can be negative due to soil heterogeneity [41]. The Green–Ampt infiltration equation was a physical model considering water flow in the unsaturated–saturated zone. The hydraulic conductivity of the soil in the partially saturated zone was strongly controlled by changes in the water potential head or suction and changes in the void ratio [35, 42]. In saturated conditions, hydraulic conductivity is a function of the void ratio or bulk density. The suction will be dominant in soil comprised of silt/clay (as at KP-4 and KP-5). Furthermore, Mishra et al. [43] mentioned that physical based model show a suitable ‘best-fitted” performance for laboratory test compared to field infiltration test. In the laboratory the circumstances can be manageable to ascertain a vertical water flow.

According to the HSG-USDA classification [44], although all soils are included in class B (see Figure 2b), they have different infiltration rate classes (see Figure 6). The soil textures can be grouped into silt-loam texture (KP-2 and KP-3) and silt texture (KP-1, KP-4, and KP-5). The infiltration rates at KP-2 and KP-3 are consistently grouped as soil with a very rapid infiltration rate. Referring to the soil particle size distribution (Figure 2a), although all soils are

classified as fine-grained soils (more than 50% have a size smaller than 0.075 mm), the soil at locations KP-2 and KP-3 contain sand fractions of 25.5% and 13%, respectively. The grain size of sand is larger than silt/clay grains, allowing the soil to have larger pore sizes. So, the water can quickly flow between the soil pores, known as diffuse flow. The soil at the KP-1 location has a sand fraction content of 13% and clay of 11% grouped as silt texture, classified in the Moderately Rapid infiltration rate class. The moderately slow to moderate infiltration rate class is at the KP-5 location, and the slow to moderately slow infiltration rate class is at the KP-4 location. The soil at the KP4 and KP-5 has a clay content of 10.8% and 12% and a sand fraction content of 11.3% and 9%. This condition indicates that soil texture and grain size distribution affect the water infiltration rate into the soil [37, 45]. Grain size distribution is closely related to soil structure, which is the arrangement of particles that form porous aggregates. The arrangement of these soil particles strongly influences the absorption and retaining of water. In soil containing more fine grain fractions (KP-4, KP-5), the pore size is smaller than in soil containing more coarse fractions (KP2, KP-3). Water flow is driven by gravitational and capillary forces resulting from the surface tension of the water-air interaction in the cavity. The forces are a function of the hydraulic pressure head or total pressure. Smaller pore sizes will hold water with greater capillary force. Thus, it is why water flows more slowly in smaller pores like clay soils. However, matric suction, total suction, or water potential do not cause water flow but determine the hydraulic conductivity [46].

The final infiltration rate is quite elusive because it is not only controlled by soil texture and structure. Several previous studies such as Ketsela et al. [30], Ruggenthaler et al. [47], Su et al. [29], Stewart et al. [42], Preez and Toerien [48], and Canarache et al. [49] conclude remarkable note on the effect of initial water content on infiltration rate. However, Stewart et al. [42] found that initial water content does not directly affect the infiltration rate but controls the total infiltrated water into the soil. In addition, higher initial soil moisture leads to time for saturation earlier to reach the final infiltration rate. The result in Table 3 indicates that the initial soil moisture affects the final infiltration rate and total infiltrated water into the soil. Figure 9 illustrates the effect of initial soil moisture on the cumulative infiltration $F(t)$, final infiltration rate f_c, and initial infiltration rate f_o. The cumulative infiltration and infiltration rate will be greater in low initial soil moisture conditions or near dry.

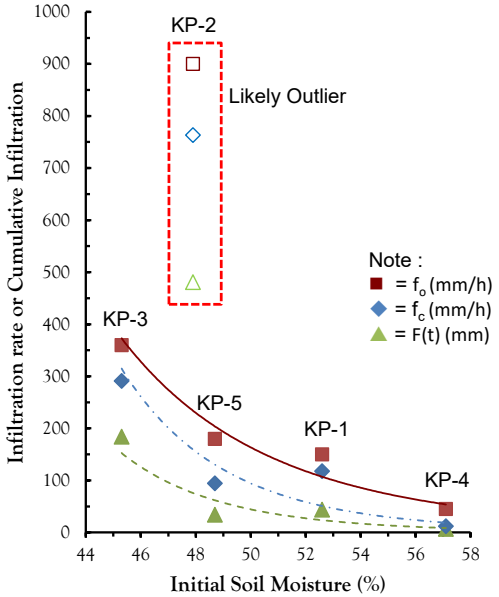

Figure 9. Relationship between Initial Soil Moisture with Cumulative Infiltration $F(T)$, Final Infiltration Rate F_c , and Intial Infiltration Rate F_o

CONCLUSIONS

The soil in this test is classified into two main groups: (1) silt – loam texture at KP-2 and KP-3, and (2) silt texture at KP-1, KP-4, and KP-5. However, the infiltration rate characteristic varies at each location. Conceptually, the double-ring infiltration test considers the water flows vertically through the voids between soil particles. The infiltration rate will decrease as the time for water to seep into the soil increases, making the soil layer wet and putting it in a saturated state so that the soil can no longer absorb water. Infiltration rates will be higher under conditions of low initial soil moisture or near dry. The boundary condition of the DRI test and soil condition (textures, moisture, structure, grain size distribution) may result in an elusive final infiltration rate. The conclusions that can be written, but these results are limited to the results of this experiment, as follows:

1. The coarse or fine fraction amount, grain size distribution, and initial soil moisture affect the infiltration rate and its derivative parameter. Based on the final infiltration rate, the silt–loam texture (KP-2 and KP-3) are consistently grouped as soil with a very rapid infiltration rate. In contrast, silt texture is classified into Very Rapid (KP-2, KP-3), Moderately Rapid (at KP-1), Moderately Slow to Moderate (KP-5), and Slow to Moderately Slow (KP-4).
2. The Horton and Kostiakov equations are derived from regression analysis based on experimental data, while Green – Ampt and Philips equations simplify the one-dimensional infiltration of the Richard's equation. The Horton and Philips infiltration model provides a better infiltration model, which results in the highest R^2 and smaller NRSME, followed by Green – Ampt and Kostiakov infiltration models.
3. The estimated hydraulic conductivity from the four infiltration models ranges 698–726 mm/h (at KP-2), 252–279 mm/h (at KP-3), and 66.9–91.9 mm/h (at KP-1). However, the hydraulic conductivity at locations KP-4 and KP-5 results in more bias, especially the estimation from the Green–Ampt and Philip infiltration models. The bias indicates the measurement constraints and the limitations of the predictor of the Green – Ampt and Philips infiltration equation.

ACKNOWLEDGMENT

This research is part of the national competitive grant entitled "The Study of the Impact of Climate Change on Slope Instability" in 2015-2017. The Ministry of Education and Culture funded the research under contract number 007/HB-LIT/III/2015 on 25 March 2015 and SP-DIPA number 023.04.1.673453/2015 on 14 November 2014. The counterpart support from the Universitas Muhammadiyah Yogyakarta is greatly appreciated through the short-term academic program in 2023 at the Disaster Prevention Research Institute, Kyoto University.

REFERENCES

1. Muntohar, A.S., Ikhsan, J., and Soebowo, E., Mechanism of Rainfall Triggering Landslides in Kulonprogo, Indonesia, in C. L. Meehan et al. (Eds.), *Geo-Congress 2013*, American Society of Civil Engineers, San Diego, California, 2013, pp. 452-461.
2. Muntohar, A.S., Fata, N., Jotisankasa, A., and Yang, K.H., Suction Monitoring and Stability of Volcanic-Residual Soil Slope during Rainfall, *Civil Engineering Dimension*, *22*(2), 2020, pp. 67-73, doi: 10.9744/CED.22.2.68-74.
3. Muntohar, A.S., Ikhsan, J., Liao, H.J., Jotisankasa, A., and Jetten, V.G., Rainfall Infiltration-induced Slope Instability of the Unsaturated Volcanic Residual Soils during Wet Seasons in Indonesia, *Indonesian Journal on Geoscience*, *9*(1), 2022, pp. 71-85, doi: 10.17014/ijog.9.1.71-85.
4. Tohari, A., Sarah, D., and Daryono, M.R., Hydrological Condition Leading to Landslide Initiation, *Media Teknik Sipil, 8*(2), 2008, pp. 67-76.
5. Ziadat, F.M. and Taimeh, A.Y., Effect of Rainfall Intensity, Slope, Land Use and Antecedent Soil Moisture on Soil Erosion in an Arid Environment, *Land Degradation & Development*, *24*(6), 2013, pp. 582-590, doi: 10.1002/ldr.2239.
6. Rahardjo, H., Ong, T.H., Rezaur, R.B., and Leong, E.C., Factors Controlling Instability of Homogeneous Soil Slopes under Rainfall, *Journal of Geotechnical and Geoenvironmental Engineering, 133*(12), 2007, pp. 1532-1543, doi: 10.1061/(ASCE)1090-0241(2007)133:12(1532).
7. Green, W.H. and Ampt, G.A., Studies on Soil Physics, *The Journal of Agricultural Science*, *4*(1), 1911, pp. 1-24, doi: 10.1017/S0021859600001441.
8. Kostiakov, A.N., On the Dynamics of the Coefficient of Water Percolation in Soils and on the Necessity for Studying It from A Dynamic Point of View for Purposes of Amelioration, in A. N. Kostiakov (Ed.), *Transactions of the Sixth Commission: Russian part, International Society of Soil Science*. Sixth Commission Soviet section, vol. 1, State Scientific Technical Publishing Office, 1932, pp. 17-21.
9. Philips, J.R., The Theory of Infiltration: 1. The Infiltration Equation and Its Solution, *Soil Science*, *83*, 1957, pp. 345-357, doi: 10.1097/00010694-195705000-00002.
10. Touma, J. and Alberge, J., Determining Soil Hydrologic Properties from Rain Simulator or Double Ring Infiltrometer Experiments: A Comparison, *Journal of Hydrology*, *135*(1-4), 1992, pp. 73-86, doi: 10.1016/0022-1694(92)90081-6.
11. D8152-18, *Standard Practice for Measuring Field Infiltration Rate and Calculating Field Hydraulic Conductivity using the Modified Philip Dunne Infiltrometer Test*, ASTM, ASTM International, West Conshohocken, Pennsylvania, USA, 2018.
12. Irmak, S., Sharma, V., Mohammed, A.T., and Djaman, K., Impacts of Cover Crops on Soil Physical Properties: Field Capacity, Permanent Wilting Point, Soil-Water Holding Capacity, Bulk Density, Hydraulic Conductivity, and Infiltration, *Transactions of the ASABE*, *61*(4), 2018, pp. 1307-1321, doi: 10.13031/trans.12700.

13. Nimmo, J.R., Schmidt, K.M., Perkins, K.S., and Stock, J.D., Rapid Measurement of Field-Saturated Hydraulic Conductivity for Areal Characterization, *Vadose Zone Journal, 8*(1), 2009, pp. 142-149, doi: 10.2136/vzj2007.0159.
14. Fatehnia, M., Tawfiq, K., and Ye, M., Estimation of Saturated Hydraulic Conductivity from Double-Ring Infiltrometer Measurements, *European Journal of Soil Science*, *67*(2), 2016, pp. 135-147, doi: 10.1111/ejss.12322.
15. Bouwer, H., Intake Rate: Cylinder Infiltrometer, in A. Klute (Ed.), *Methods of Soil Analysis: Part 1 Physical and Mineralogical Methods*, American Society of Agronomy Inc., Soil Science Society of America Inc. Publisher, Madison, Wisconsin USA, 1986, pp. 825-844.
16. Yolcubal, I., Brusseau, M.L., Artiola, J.F., Wierenga, P., and Wilson, L.G., Environmental Physical Properties And Processes, in J. F. Artiola et al. (Eds.), *Environmental Monitoring and Characterization*, Academic Press, Burlington, 2004, pp. 207-239.
17. Wahyu, P., Sri Malahayati, Y., and Enny Dwi, W., Study of Two Different Field Measurement Methods of Infiltration: Falling Head and Constant Head, at Various Hydraulic Head, *Jurnal Ilmu Tanah dan Lingkungan*, *26*(1), 2024, pp. 54-59, doi: 10.29244/jitl.26.1.54-59.
18. Octariko, M.N. and Budianta, W., *The Study of Soil Infiltration in West Part of Semarang City, Indonesia,* The 2nd Geoscience and Environmental Management Symposium, Yogyakarta, Indonesia, in R. Che Omar et al. (Eds.), September 7-8 2021, vol. 325: E3S Web of Conferences doi: 10.1051/e3sconf/202132502007.
19. Dou, H.Q., Han, T.C., Gong, X.N., and Zhang, J., Probabilistic Slope Stability Analysis Considering the Variability of Hydraulic Conductivity under Rainfall Infiltration–Redistribution Conditions, *Engineering Geology, 183*, 2014, pp. 1-13, doi: 10.1016/j.enggeo.2014.09.005.
20. Wisaksono, B., Slope Stability Analysis Causing Ground Movement at Kalibawang Irrigation Main Channel Km. 15,9 in Kulonprogo, Master Thesis, Department of Civil Engineering, Universitas Gadjah Mada, Yogyakarta, 2003. (in Indonesian)
21. Ma'ruf, B., Geometry Pattern of Soil Creep in Segment Km.15.9 of Kalibawang Irrigation Main Channel in Kulonprogo using Kalman Filtering Method, Ph.D. Dissertation, Department of Geological Engineering, Universitas Gadjah Mada, Yogyakarta, 2015. (in Indonesian)
22. Muntohar, A.S. and Saputro, R.I., The Effect of Initial Grounwater Level on the Stability Analysis of Unsaturated Slopes, *Proceeding Seminar Nasional X – 2014 Teknik Sipil ITS Surabaya*, 5 Februari 2014, pp. 985-990. (in Indonesian)
23. USDA-NRCS, Engineering Classification of Earth Materials, *National Engineering Handbook, Part 631: Geology Uniter State Department of Agriculture,* National Resources Conservation Services, Washington D.C., USA, 2022.
24. D3385-09, *Standard Test Method for Infiltration Rate of Soils in Field Using Double-Ring Infiltrometer*, ASTM, ASTM International, West Conshohocken, PA, USA, 2009.
25. SNI 1965-2008, Test Method for Determining Water Content for Soil and Rock, National Standardization Agency, Jakarta, Indonesia, 2008. (in Indonesian)
26. Horton, R.E., An Approach toward a Physical Interpretation of Infiltration-Capacity, *Soil Science Society of America Journal*, *5*, 1940, pp. 399-417, doi: 10.2136/sssaj1941.036159950005000C0075x.
27. Marquardt, D.W., An Algorithm for Least-Squares Estimation of Nonlinear Parameters, *Journal of the Society of Industrial and Applied Mathematics, 11*(2), 1963, pp. 431-441.
28. Mentaschi, L., Besio, G., Mazzino, A., and Cassola, F., Why NRMSE is not Completely Reliable for Forecast/hindcast Model Test?, *Geophysical Research Abstracts*, *15*, 2013, pp. EGU2013-7059.
29. Su, L., Wang, Q., Shan, Y., and Zhou, B., Estimating Soil Saturated Hydraulic Conductivity using the Kostiakov and Philip Infiltration Equations, *Soil Science Society of America Journal*, *80*(6), 2016, pp. 1463-1475, doi: 10.2136/sssaj2016.04.0125.
30. Ketsela, Y.S., Hatiye, S.D., and Muche, A.T., Evaluating the Effect of Initial Soil Moisture Content on Infiltration Characteristics using Empirical and Hydrus 1D Models, *Water Conservation Science and Engineering*, *8*(1), 2023, doi: 10.1007/s41101-023-00216-w.
31. Mesele, H., Grum, B., Aregay, G., and Berhe, G.T., Evaluation and Comparison of Infiltration Models for Estimating Infiltration Capacity of Different Textures of Irrigated Soils, *Environmental Systems Research, 13*(1), 2024, doi: 10.1186/s40068-024-00356-5.
32. Bodman, G.B. and Colman, E.A., Moisture and Energy Conditions during Downward Entry of Water Into Soils, *Soil Science Society of America Journa*l, *8*(C), 1944, pp. 116-122, doi: 10.2136/sssaj1944.036159950008000C0021x.
33. Yao, M., Chen, T., Wei, X., Tao, W., Fan, R., and Liu, J., Wetting Front Expansion Model for Non-Ponding Rainfall Infiltration in Soils with Uniform and Non-Uniform Initial Moisture Content, *Applied Sciences*, *12*(12), 2022, doi: 10.3390/app12126185.

34. Brunone, B., Ferrante, M., Romano, N., and Santini, A., Numerical Simulations of One-Dimensional Infiltration into Layered Soils with the Richards Equation Using Different Estimates of the Interlayer Conductivity, *Vadose Zone Journal*, *2*(2), 2003, pp. 193-200, doi: 10.2136/vzj2003.1930.
35. Vogel, H.J., Gerke, H.H., Mietrach, R., Zahl, R., and Wöhling, T., Soil Hydraulic Conductivity in the State of Nonequilibrium, *Vadose Zone Journal, 22*(2), 2023, doi: 10.1002/vzj2.20238.
36. Ma, Y., Feng, S., Su, D., Gao, G., and Huo, Z., Modeling Water Infiltration in a Large Layered Soil Column with a Modified Green–Ampt Model and HYDRUS-1D, *Computers and Electronics in Agriculture, 71*, 2010, pp. S40-S47, doi: 10.1016/j.compag.2009.07.006.
37. Berdouki, A.A., Besharat, S., Zeinalzadeh, K., and Cruz, C., The Effect of Soil Texture, Layering and Water Head on the Infiltration Rate and Infiltration Model Accuracy, *Irrigation and Drainage*, *73*(3), 2024, pp. 846-865, doi: 10.1002/ird.2918.
38. Lai, J., Luo, Y., and Ren, L., Numerical Evaluation of Depth Effects of Double-Ring Infiltrometers on Soil Saturated Hydraulic Conductivity Measurements, *Soil Science Society of America Journal*, *76*(3), 2012, pp. 867-875, doi: 10.2136/sssaj2011.0048.
39. Zhang, Y., Zhang, Z., Ma, Z., Chen, J., Akbar, J., Zhang, S., Che, C., Zhang, M., and Cerdà, A., A Review of Preferential Water Flow in Soil Science, *Canadian Journal of Soil Science*, *98*, 2018, pp. 604–618, doi: 10.1139/cjss-2018-0046.
40. Mbagwu, J.S.C., Soil Physical Properties Influencing the Fitting Parameters in Philip and Kostiakov Infiltration Models, *International Atomic Energy Agency and UNESCO International Centre for Theoretical Physics*, Miramare,Trieste, Italy., Internal Report IC/94/97, 1994.
41. Regalado, C.M., Ritter, A., Álvarez-Benedí, J., and Muñoz-Carpena, R., Simplified Method to Estimate the Green–Ampt Wetting Front Suction and Soil Sorptivity with the Philip–Dunne Falling-Head Permeameter, *Vadose Zone Journal*, *4*(2), 2005, pp. 291-299, doi: 10.2136/vzj2004.0103.
42. Stewart, R.D., Rupp, D.E., Najm, M.R.A., and Selker, J.S., Modeling Effect of Initial Soil Moisture on Sorptivity and Infiltration, *Water Resources Research*, *49*(10), 2013, pp. 7037-7047, doi: 10.1002/wrcr.20508.
43. Mishra, S.K., Tyagi, J.V., and Singh, V.P., Comparison of Infiltration Models, *Hydrological Processes*, *17*(13), 2003, pp. 2629-2652, doi: 10.1002/hyp.1257.
44. USDA-NRCS, Hydrologic Soil Groups, *National Engineering Handbook Part 630: Hydrology,* United States Department of Agriculture, Natural Resources Conservation Service, Washington DC, USA, 2009.
45. Zarooei, F. and Fereidooni, D., Assessing the Effect of Particle Size Distribution on Permeability of Silty-Sandy Soils, *Geotechnical and Geological Engineering*, *41*(6), 2023, pp. 3681-3698, doi: 10.1007/s10706-023-02481-x.
46. Zhan, T.L.T., Ng, C.W.W., and Fredlund, D.G., Field Study of Rainfall Infiltration into a Grassed Unsaturated Expansive Soil Slope, *Canadian Geotechnical Journal*, *44*(4), 2007, pp. 392-408, doi: 10.1139/t07-001.
47. Ruggenthaler, R., Meißl, G., Geitner, C., Leitinger, G., Endstrasser, N., and Schöberl, F., Investigating the Impact Of Initial Soil Moisture Conditions on Total Infiltration by Using An Adapted Double-Ring Infiltrometer, *Hydrological Sciences Journal,* 2016, pp. 1-17, doi: 10.1080/02626667.2015.1031758.
48. Preez, D.F.D. and Toerien, J.C., The Influence of Initial Soil Moisture Content on Field Measured Infiltration Rates, *Water SA*, *4*(1), 1978, pp. 18–24, doi: 10.10520/AJA03784738_2137.
49. Canarache, A., Motoc, E., and Dumitriu, R., Infiltration Rate as Related to Hydraulic Conductivity, Moisture Deficit and Other Soil Properties, in P. E. Rijtema & H. Wassink (Eds.), *Water in the Unsaturated Zone: Proceedings of the Wageningen Symposium,* vol. 1, 1969, pp. 392-401.